AIAA JOURNAL
Vol. 48, No. 10, October 2010

High-Bandwidth Pulsed Microactuators for High-Speed Flow Control

John T. Solomon,* Rajan Kumar,† and Farrukh S. Alvi‡
Florida A&M and Florida State University, Tallahassee, Florida 32310

DOI: 10.2514/1.J050405

A systematic study on the design, development, and characterization of high-momentum, high-bandwidth microactuators for high-speed flow control is described in this paper. Beginning with building-block experiments, multiple resonant flow phenomena are used in the actuator design to arrive at an actuator configuration that provides the desired flow properties. The first-generation actuator design consists of an underexpanded source jet incident upon a cavity. The lower surface of this cavity contains micronozzles through which the unsteady microjets (400 μm) issue. Results show that microjets produced by this actuator have a high mean momentum (300–400 m/s) and a significant unsteady component (20–30% of the mean). Experiments were conducted over a large range of parameters in terms of cavity length, source jet nozzle pressure ratio, and impingement distance. The results unequivocally demonstrate the ability to vary the frequency and the amplitude of the mean and unsteady momentum of microjets issuing from this actuator. By varying the dimensions of the actuator by few hundred microns and/or source jet pressure by roughly 1 atm, one is able to vary the frequency rather precisely over a range of 5–20 kHz. A correlation based on Strouhal number and jet column length is suggested for the design of actuators. Actuators in the frequency range of a few to well over 50 kHz have been designed and characterized. It is believed that the frequency range may be extended down to $\mathcal{O}$(100 Hz) and up to $\sim\mathcal{O}$(100 kHz) using this actuator approach.

I. Introduction

DESIGN and development of active flow control systems have received wide attention in the recent years due to their ability in reducing or eliminating a number of adverse and parasitic effects associated with aerodynamic flow and providing potentially substantial gains in performance. A number of such systems have been developed and tested over the years by many researchers, some of which were found promising in a limited range of flow conditions. Ideally, the desired control effect (e.g., noise reduction, flow separation control, and turbulent mixing) must be achieved with minimal energy input. Active control of high-speed flow demands high-amplitude and high-bandwidth actuation techniques for the effective and efficient manipulation of such high-energy/high-momentum flows and structures that are often responsible for the adverse flow characteristics. An example of such a flowfield is associated with a supersonic cavity. Various active and passive control strategies have been explored to control the aeroacoustically induced cavity flow oscillations (Zhuang. et al. [1] and Ukeiley et al. [2]). Another high-speed flowfield that requires proficient active control is associated with supersonic impinging jets (Krothapalli et al. [3], Alvi et al. [4], and Kumar et al. [5]). A short takeoff and vertical landing aircraft during its hovering mode, especially in close proximity to the ground, produces a highly unsteady flowfield that produces intense unsteady aeroacoustic loads that can lead to ground erosion and structural damage to the near-field structures. The above examples point to the necessity of developing energy-efficient and effective actuator systems for a number of aeroacoustic problems. In addition, progress in the area of microelectronics has given rise to more challenging problems associated with the thermal management of microdevices (Ro and Loh [6]). Development of effective microactuator systems that are scalable and capable of addressing some of these issues may potentially be beneficial toward solving these problems as well.

Flow control methods are generally classified into active and passive based on the involvement of external energy in the control process. Passive methods do not require external energy input but make use of the energy associated with the primary flow for the purpose of control. Variations in nozzle geometry, i.e., rectangular, triangular, elliptic, etc. (Sfeir [7], Sforza et al. [8], and Schadow et al. [9]), use of mechanical tabs of different shapes and the use of splitter plates (Zaman et al. [10] and Reeder and Samimy [11]) are examples of various passive control methods adopted for the control of jet noise. On the other hand, in active flow control schemes, an external energy source is used for tailoring the natural behavior of a shear-layer or a boundary-layer flow according to the control objectives. The ability to efficiently adapt to changing flow conditions (the ultimate goal of active control schemes) makes them more attractive than passive methods.

Mechanical systems such as vibrating ribbons and cantilevered beams and electromechanical devices such as piezoelectric diaphragms, voice coils, and speakers are used as external energy sources in various active flow control schemes. The vibration of a piezoelectric material is used for generating a low-momentum air jet with zero net mass flux (synthetic jets) for the control of cavity flows (Cattafesta et al. [12]) and shear flows (Wiltse and Glezer [13]). Actuators based on synthetic jets have also been used for separation control over airfoils and cylinders (Amitay et al. [14]). A number of researchers in the past modified the Hartmann tube and used it as a flow actuator, demonstrating reasonable success over a limited range of flow conditions (Raman and Kibens [15], Kastner and Samimy [16], and Dziuba and Rossmann [17]). Although relatively successful at low speeds, many actuators are not very efficient when the primary flow velocities are high, in particular supersonic. Optimal manipulation of the shear or boundary layer of high-speed flows requires aeroacoustic disturbances with high momentum or energy, and actuators whose steady and unsteady components can be manipulated. A simple and robust actuator, with high mean and unsteady momentum that can be easily integrated into practical high-speed flow applications and subsystems is essential for efficient active flow control schemes. The present studies are motivated and driven by this goal.

Presented as Paper 2008-3042 at the 14th AIAA/CEAS Aeroacoustics Conference, Vancouver, British Columbia, Canada, 5–7 May 2008; received 28 December 2009; revision received 21 May 2010; accepted for publication 8 June 2010.

*Graduate Research Assistant, Florida Center for Advanced Aeropropulsion, Department of Mechanical Engineering. Student Member AIAA.

†Research Scientist, Florida Center for Advanced Aeropropulsion, Department of Mechanical Engineering. Senior Member AIAA.

‡Professor, Florida Center for Advanced Aeropropulsion, Department of Mechanical Engineering. Associate Fellow AIAA.

Over the last decade, supersonic impinging-jet flows have been the subject of extensive study at our laboratory. To reduce the feedback-driven unsteadiness in the impinging-jet flowfield, an array of *supersonic steady microjets*, were mounted circumferentially around the main jet. This control technique proved to be very effective, reducing the overall pressure fluctuations and noise levels by as much as 10–15 dB for cold and hot impinging jets. One of the reasons for the success of this technique is likely due to the fact that the high momentum associated with the supersonic microjets allows them to penetrate the primary jet shear layer sufficiently to disrupt the feedback loop (Alvi et al. [4], Kumar et al. [5], and Lou et al. [18]). Furthermore, the small diameter of the supersonic microjets dramatically reduces the mass flow requirement while producing very high-momentum jets. This microjet-based control scheme was equally successful when applied for reducing the unsteady pressure loads in a supersonic cavity flow (Zhuang et al. [1]). The pressure spectra depicting the effect of microjet control on a supersonic impinging jet (Kumar et al. [5]) and supersonic cavity flow (Zhuang et al. [1]) are shown in Fig. 1.

These spectra show the presence of strong, discrete tones in the baseline flow approximately in the range of 4–10 kHz. With steady microjet control, the amplitude of the tones was reduced significantly but not completely eliminated. It is anticipated that actuators with a strong unsteady component in this frequency range could further enhance the control efficacy of microjet-based control of such flows. Motivated by the success of steady supersonic microjets for flow control, and the lessons learned from our previous research and those of others, a program was initiated to develop *pulsed microjet actuators* that produce unsteady microjets with high mean and unsteady momentum and whose actuation frequency would be variable over a large range. Here, we describe an experimental program, where high-speed microjets are combined with a cavity and other geometric features to generate a highly unsteady, pulsed flow. Such a flow could be used to produce high-momentum, unsteady jets, which can be used as fluidic actuators. Furthermore, the unsteady component (frequencies) of such actuators can be tuned for specific applications.

II. Experimental Apparatus and Procedures

The experiments were conducted in the Advanced Aero-Propulsion Laboratory at the Florida State University. Measurements include flowfield visualization using a lens-based microschlieren system and unsteady pressure measurements using an ultraminiature Kulite pressure transducer. Measurements were made for the actuator source jet operating over a range of nozzle pressure ratios (NPR) equal to jet stagnation pressure/ambient pressure of 1.9–6.8, corresponding to moderate to strongly underexpanded jets and over a range of geometrical parameters. The details of the measurement techniques employed are described below.

A. Microschlieren System

Since the length scales associated with the present actuator system are too small ($\sim$10 μm) to be resolved by a conventional schlieren system, a specifically designed lens-based microschlieren system (similar to the one used in Phalnikar et al. [19]) with very high magnification and sensitivity is used for the present study. The flowfield is visualized at an optimized combination of the critical parameters that determine the quality of the schlieren images, such as magnification, resolution, field of view, and sensitivity. The microschlieren system uses high-magnification, in-line achromatic lens-based optics, coupled with a graded filter (to minimize diffraction effects) and a Kodak Megaplus ES 1.0 camera with a charge-coupled-device array of resolution of 1008 $\times$ 1018 pixels. A white light stroboscopic lamp with adjustable frequency (up to 1 kHz) and intensity was used as the light source. The resultant magnification obtained from the lens-based system was as high as 4–5. More details of the optics used in the microschlieren system are available in Phalnikar et al. [19].

B. Unsteady Pressure Measurements

The unsteady flow issuing out of these microjets was measured using a probe (1.5 mm diameter) with a 100 psia range, ultra-miniature (1.3 mm diameter) Kulite model XCE-062 pressure transducer. The unsteady pressure signals were acquired through high-speed National Instruments digital data acquisition cards using LabVIEW software. The transducer output was conditioned using a low-pass Stanford SR640 filter (cutoff frequency of 60 kHz) and sampled at 200 kHz. Standard DFT (discrete Fourier transform) analysis was used to obtain narrowband pressure spectra using 4096 points/DFT. A total of 100 DFTs so computed, without overlap, were averaged to obtain statistically reliable narrowband spectral estimates.

C. Measurement Uncertainties

The important geometrical and flow parameters involved in the present study are the nozzle to cavity distance h, length of the cavity L and the nozzle pressure ratio NPR. The cavity length L was machined with tolerances of $\pm$10 microns. Precise measurement of h during experiment was achieved using microtraverses with an accuracy of $\pm$12.5 microns. The pressure sensors used for these experiments were carefully calibrated. An Omega transducer PX303-200 G5V was used to measure jet total pressure and the uncertainty associated with the total pressure measurement was $\pm$1 psi. The unsteady pressure measurements made using the Kulite sensor were accurate within $\pm$0.1 psi.

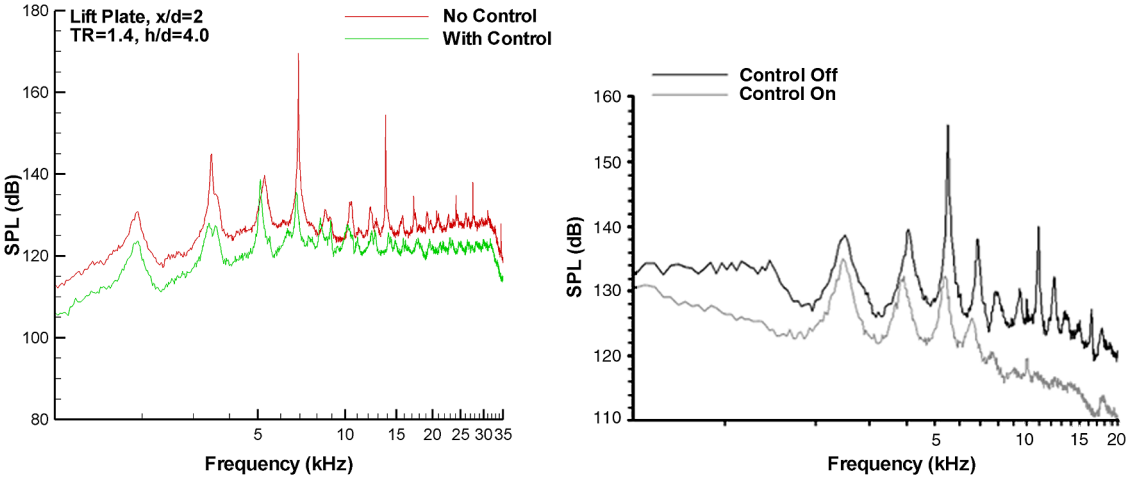

a) Mach 1.5 Impinging jet (Kumar et al. [5]) b) Mach 2 Cavity flow (Zhuang et al. [1])

Fig. 1 Pressure spectra illustrating the effect of steady microjet control of supersonic flows.

III. Building-Block Experiments for Microactuator Development

The initial inspiration for this actuator design came from our extensive studies of larger supersonic impinging jets (Krothapalli et al. [3] and Alvi et al. [4]). As seen in Fig. 1a, such jets produce a highly unsteady flowfield with significant energy at discrete frequencies, seen as high-amplitude peaks in Fig. 1 and commonly referred to as impingement tones. Furthermore, the frequency of these tones can be varied by varying the jet NPR and/or the distance between the nozzle and the impingement surface. Our studies of steady microjets, which were used to control the larger impinging jets, revealed the striking similarities in the mean flow properties between the larger impinging jets and impinging microjets (Phalnikar et al. [19]). Given these similarities, the question was asked whether the unsteady flow properties of *impinging microjets* are also similar to their larger counterparts: i.e., do they produce highly unsteady, discrete frequency-dominated flowfields? If so, then one may possibly use these as a basis for a high control authority, tunable, unsteady actuator. This initial idea led to the development of the present pulsed microjet-based actuators in a systematic process involving building-block experiments and the methodical addition of design elements to produce the first-generation actuator. In this section, we briefly discuss some initial experiments that were conducted using simple canonical configurations. The aim of these studies was to gain some insight and guidance toward the design of the final pulsed microactuators, which is discussed later in Sec. IV.

A. Supersonic Impinging Microjets

As discussed above, large scale supersonic impinging jets produce highly unsteady flowfields that exhibit discrete acoustic tones of high intensity (Powell [20] and Krothapalli et al. [3]). The impinging-jet flowfield of a microjet is examined as a first step to understand how the microscaling of the geometry and the resulting lower Reynolds numbers affect this unsteadiness. Figure 2 shows the configuration and narrow band pressure spectra of a microjet impinging on a flat surface for various nozzle-to-plate h_i/d distances, where h_i is the distance between the nozzle exit plane and the impingement surface, and d is the nozzle diameter at the throat. The jet is moderately underexpanded (NPR = 5.8) and impinging on a flat surface normal to the jet axis. A Kulite sensor is flush mounted to measure the unsteady surface pressures. The narrow band spectra shown above demonstrate the presence of high-amplitude, discrete tones in the frequency range of 25–55 kHz over the range of h_i/d (1.8 to 2.8) tested.

These results confirm the presence of a resonance loop, as observed for larger impinging jets, and suggest that this property may be leveraged for our actuator development. However, due to the small physical scales, the frequency range of these tones is much higher than those required for the development of microactuator for our applications (see Fig. 1). Hence, a modification to the impinging-jet configuration is needed to produce unsteady microjets in the desired frequency range.

B. Microjets with Hole Tones

The unsteady flowfield characteristics of edge/hole tones and the effect of various geometric parameters have been studied in detail by Powell [21] for larger jets. To leverage the understanding gained from prior research, experiments were conducted on microjets grazing through a circular hole. In the present study, a 1 mm diameter d jet and a sharp-edged orifice of 1.6 mm diameter D was used (Fig. 3a). Given that the feedback mechanisms in governing impinging jets, screeching jets, and hole tones are very similar (see Krothapalli et al. [3]), the geometry was designed such that the shear layer of the microjet grazes the edges of the circular hole to generate large-amplitude tones, often referred to as hole tones. We chose a $D/d = 1.6$ based on the previous studies (Phalnikar et al. [19]) on microjet impingement and its shear-layer growth to ensure such grazing flow. A Kulite probe located at a distance of $5d$ from the orifice was used for the unsteady pressure measurement.

As seen in the pressure spectra (Fig. 3b), the presence of the orifice has increased the overall unsteadiness in the jet by about 6 dB, in comparison with a free jet under the same conditions. The maximum unsteadiness in the jet is observed when the orifice is located at $h_o/d = 1.3$, where h_o is the distance from the source jet nozzle exit to the orifice. The interaction of the shear layer with the orifice edge leads to an amplification of the flow instabilities and the resulting pressure fluctuations may lead to resonance and a global unsteadiness in the flow. This behavior may be leveraged for the actuator design. Combining the configurations discussed above and adding little more geometric complexity, the impinging characteristics of a jet in a short cavity was investigated, as discussed next.

C. Microjets in a Cavity

Motivated by above results for microjets and the well-known characteristics of a Hartmann tube [22], we next explored the unsteady flowfield of microjets impinging in a cylindrical cavity. The results corresponding to a 1 mm diameter jet normally incident in a cylindrical cavity of length $L = 4.7$ mm and diameter $D = 1.4$ mm

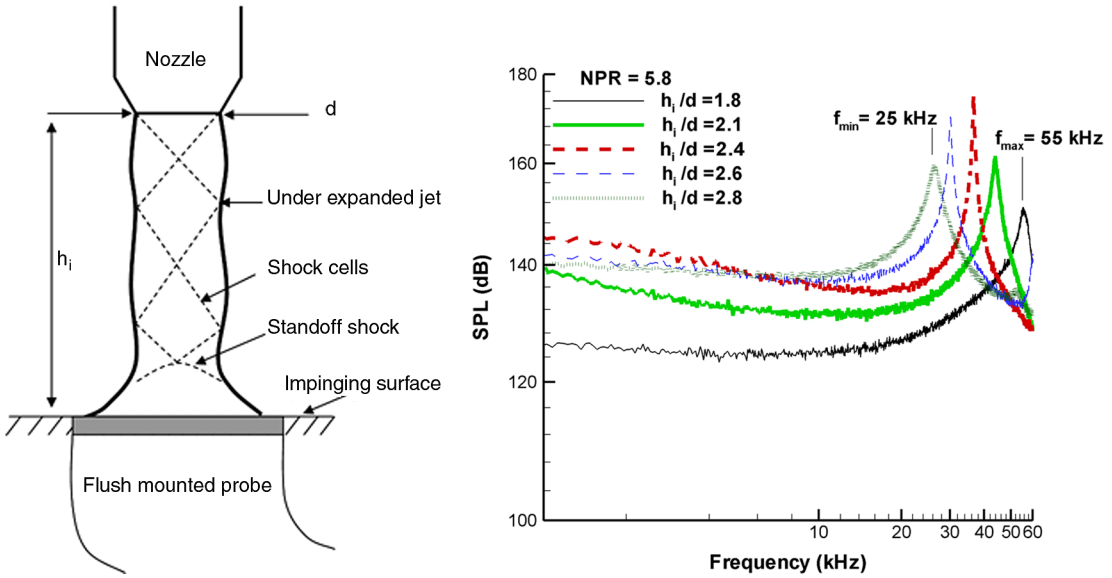

a) Configuration **b) Unsteady pressure spectra**

Fig. 2 Impinging-microjet (1 mm) configuration and corresponding pressure spectra at various impingement distances h_i/d.

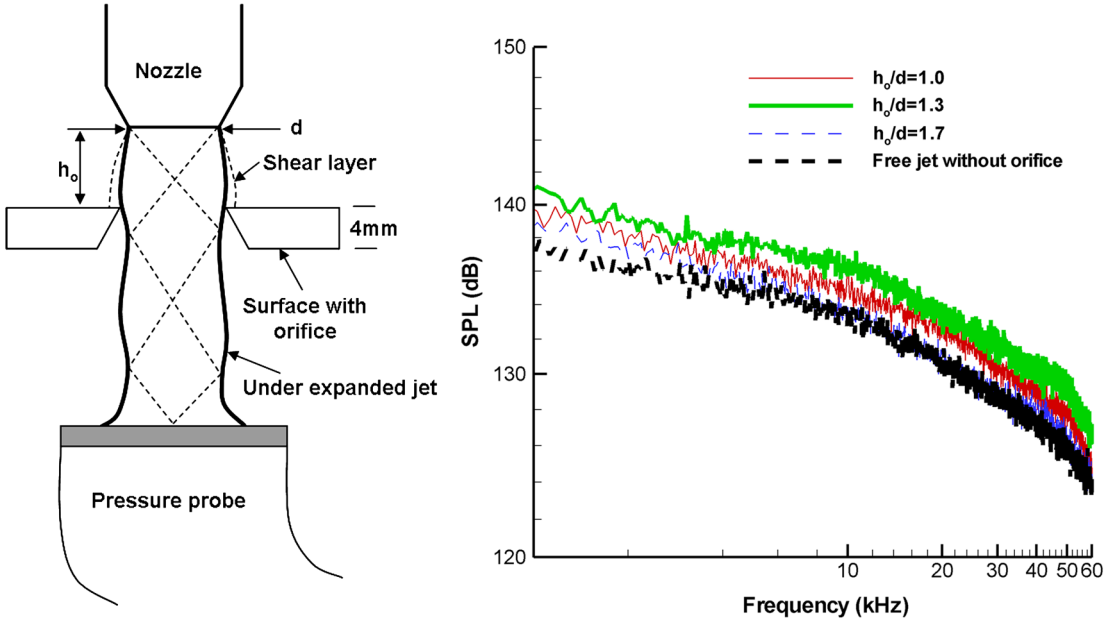

a) Configuration b) Unsteady pressure spectra

Fig. 3 Microjet–orifice configuration and corresponding pressure spectra at various impingement distances h_o/d.

are presented here. Figure 4a shows a schematic of this arrangement and the corresponding pressure spectra produced for microjets impinging into this cavity over a range of NPR (1.9–6.3) for a fixed nozzle to cavity distance $h_c = 1.6$. As seen here, the spectra (Fig. 4b) show distinct high-amplitude peaks (or tones) in the frequency range of 6–11 kHz for an NPR range of 4.1–6.3 for this configuration. These results were very encouraging both in terms of the high amplitudes and the associated tonal frequency range, which lies in the range needed for the lab-scale supersonic cavity and impinging-jet control applications (see Fig. 1). The experimental results discussed so far form the basis for a preliminary design of an actuator system that can provide high-momentum microjets with significant unsteady amplitudes, whose frequency can be varied. The design of a microactuator system and experimental results using this system are discussed in the following.

IV. Pulsed Microactuator Design

The results of the building-block experiments described in the previous section are very encouraging. They provide ample evidence of the potential to produce unsteady, high-momentum microjets by expanding upon the simple canonical configurations shown in Figs. 2–4. Based on these results a first-generation microactuator was designed, a schematic of which is shown in Fig. 5. The microactuator consists of three main components: 1) A larger, underexpanded *primary source jet*, which supplies air to 2) a *cylindrical cavity* in which the source jet resonates, and 3) multiple *micronozzles* (i.e., microjet orifices) at the bottom of the cylindrical cavity, from which the high-momentum, *unsteady microjets* issue.

In the present design, the source jet issued from a 1-mm-diam converging nozzle and the micronozzle array at the bottom of the cavity consists of four 400 μm micronozzles in the pattern shown in

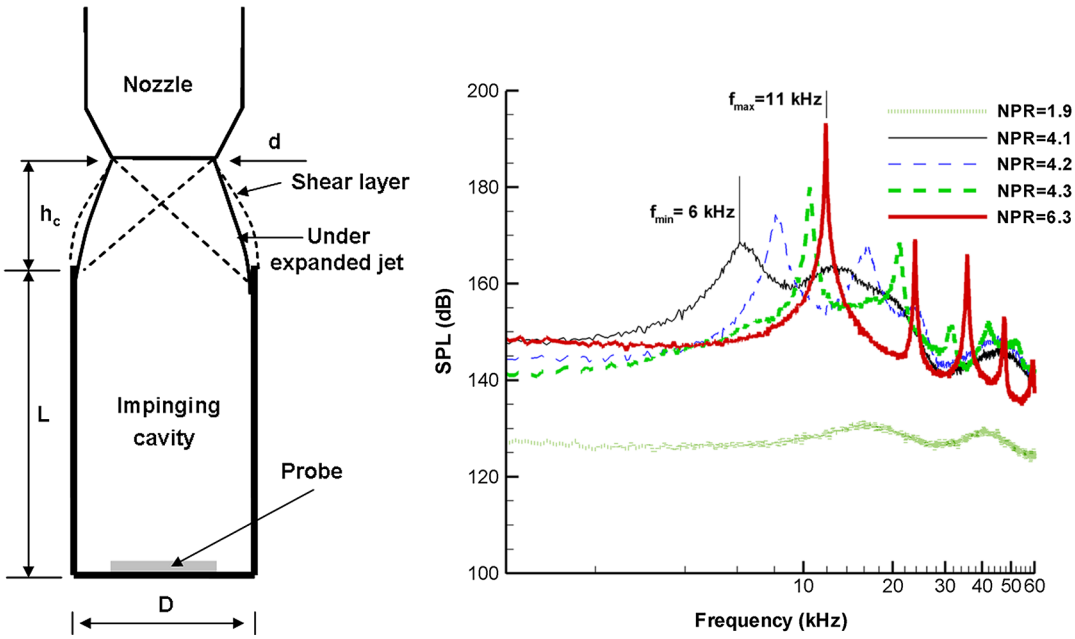

a) Configuration b) Pressure spectra

Fig. 4 Microjet–cavity configuration and corresponding pressure spectra at various NPR.

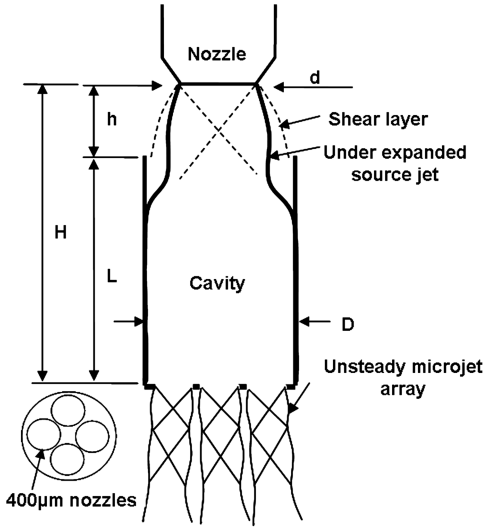

Fig. 5 Schematic of microactuator.

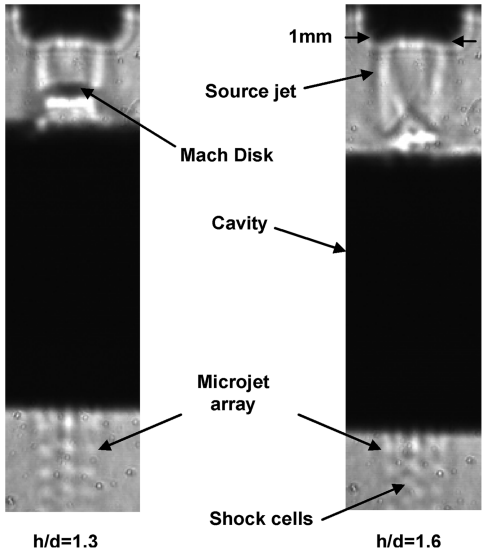

Fig. 6 Schlieren images of the flowfield at NPR = 4.8 and $L/d = 3$.

Fig. 5. The aim was to obtain the maximum flow rate through this actuator and four was maximum number of orifices that could be machined in the present configuration. (We have subsequently explored alternate cavity designs that allowed for a larger number of orifices and a corresponding increase in flow rate; the results of these ongoing studies will be published separately, once the experiments are completed.) As previously mentioned, the cavity diameter D (1.6 mm, kept constant in this study) was chosen such that the shear layer of the source jet grazes the lip/entrance of the orifice. The unsteady microjet flow was visualized using the high magnification microschlieren system discussed in Sec. II.A. The flow properties of the microjets were measured using a Kulite total pressure probe, fabricated using a Kulite XCE-062-100A (100 psia) transducer. Given the very small size of the microjets ($\sim$0.016 in.) some spatial averaging will undoubtedly occur. However, as discussed later, measurements made with the probe tangential to (i.e., grazing the unsteady microjet plume) confirm that the unsteady properties discussed in the following represent the overall unsteady microjet behavior.

V. Actuator Flowfield Properties

The main parameters that govern the flow properties of the microjet array issuing from the actuator assembly are: a) the distance from the source jet h, b) the length of the cylindrical cavity, L and c) the source jet pressure ratio, NPR. Experiments were conducted over a wide range in terms of geometric and flow parameters, where h/d is varied from 1 to 2, L/d from 1 to 5 and NPR from 1.9 to 6.3. The objective was to examine and understand the effect of these parameters on the flowfield issuing from the actuator array and to identify the optimal range and combination of these parameters that produce the desired microactuator flow. Furthermore, we aim to develop a preliminary design approach and scaling laws for such actuators. In subsequent discussion, the flowfield characteristics and the unsteady properties of the secondary microjets are presented as these parameters are varied.

A microschlieren system was extensively used to understand the flow features of the microactuator throughout the development process. In fact, a significant amount of insight into the flow physics involved in the microactuator system is gained from these images. Figure 6 shows representative instantaneous schlieren images of the flowfield associated with a microactuator at NPR = 4.8 for two values of h/d (1.3 and 1.6).

At $h/d = 1.3$, large oscillations of the Mach disc (see Fig. 6) of the primary jet at the entrance of the cavity were observed, which led to a strong tone in the pressure spectra, presented in the next section. There were no visually observable oscillations in the flow at $h/d = 1.6$, a property confirmed by the corresponding pressure spectra being devoid of any discrete tones (shown later). The presence of shock cells in the microjets issuing from the bottom of the actuator clearly confirms that the flow is supersonic. The flowfield for $h/d = 1.3$ is further analyzed in Fig. 7, in which we show images corresponding to different phases of flow oscillation. One interpretation of these images based on the shock structure of the source jet and the strength of microjets is as follows. As the primary jet fills up the cavity (Fig. 7a); flow oscillates in the cavity, where it appears to move up as in Figs. 7b and 7c and down as in Fig. 7d, and is discharged through orifices producing highly unsteady microjets. Similar flow features were observed at other test conditions in which the level of unsteadiness in the flow was dependent upon the geometric and flow parameters of the actuator.

As mentioned earlier, the geometric parameters involved in the microactuator flow are the distance from the source jet h and the length of the cylindrical cavity, L and the flow parameter is the source jet pressure ratio, NPR. In the subsequent sections, we present results based on the nondimensionalized quantities, L/d and h/d, which also represent control knobs in the microactuator performance. These parameters were systematically varied to better understand their influence on microactuator flow properties from which to formulate the design criteria.

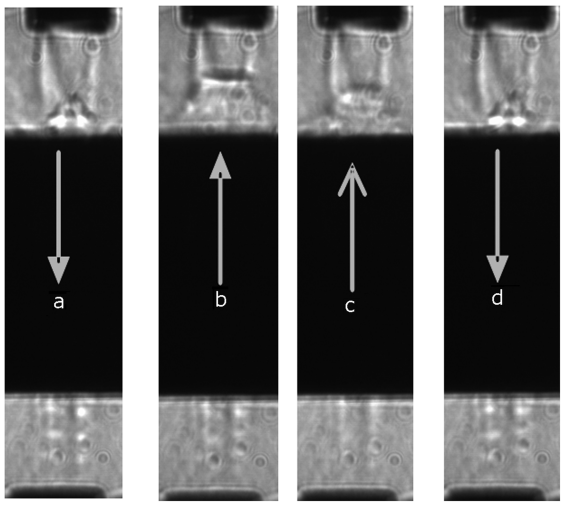

Fig. 7 Schlieren images of various phases of flow oscillations at $h/d =$ 1.3 and NPR = 4.8.

VI. Microactuator Frequency Properties: A Parametric Study

The pressure spectra of the flow issuing from the microjet actuators for a cavity length $L/d = 1$ is shown in Fig. 8. Figure 8a shows the effect of varying h/d while NPR is kept constant (NPR = 4.8), and Fig. 8b shows the effect of varying the NPR for a fixed value of $h/d = 1.4$. Unless otherwise noted, all subsequent pressures shown were measured using the Kulite probe described in Sec. III.

The spectra in both figures clearly show the presence of high-amplitude peaks indicating the presence of highly unsteady flow issuing from the actuators. Equally noteworthy is the trend in the peak frequency variation seen in Fig. 8a, in which a modest variation of h/d (from 1.3 to 2) leads to a significant shift in the peak frequency. For example, at $h/d = 1.3$ a spectral peak with an amplitude of ~157 dB occurs at a frequency of approximately 58 kHz, whereas at $h/d = 1.8$ the peak has shifted to a lower frequency of ~42 kHz and with an amplitude of roughly 141 dB. Furthermore, the spectral peaks systematically broaden with increasing h/d and beyond $h/d = 1.8$, there is no measurable discrete peak. The presence of narrow spectral tones is expected as this actuator design leverages a number of flow-acoustic resonance phenomena to enhance the flow unsteadiness; some of these have already been discussed in Sec. III. Similarly, the shift to lower frequencies with increasing spatial lengths or distances is also expected. Likewise, if one is using impinging-jet resonance, then the feedback loop governing such phenomenon is expected to become weaker beyond some critical distance due to the decay in the strength of the flow instabilities. For the present case, this critical distance appears to be $h/d = 2$, which may be due to the fact that only the shear layer is impinging/grazing the cavity lip while the core of the jet enters the cavity. A variation in NPR also produces a shift in peak frequency (Fig. 8b): at NPR = 4.5, the high-amplitude tone is at approximately 51 kHz, whereas at NPR = 4.8, it is shifted to 54 kHz. It is to be noted that a minimum jet pressure is required to produce high-amplitude tones; in the present case this corresponds to NPR > 4.2. This issue is further discussed in Sec. VIII.

The results in Fig. 8 are promising in that they clearly show the capability of this actuator to produce highly unsteady flow. Equally important, we see the presence of simple control knobs (namely, NPR and h/d), which allows one to vary the frequency and amplitude of the unsteady flow from these actuators. Keeping in mind that the two applications in which we first plan to implement and test such actuators in our laboratory, i.e., the supersonic impinging jet and cavity flowfield, require frequencies in a range of 6–10 kHz (see Fig. 1), we next examine ways of reducing the unsteady frequencies to this range.

Figures 9 and 10 show pressure spectra for longer cavities: $L/d =$ 2 and 3, respectively. The trends observed are very similar to the one with $L/d = 1$ except that the output frequency range is shifted to lower values. As seen in Fig. 9, for $L/d = 2$, an h/d variation from

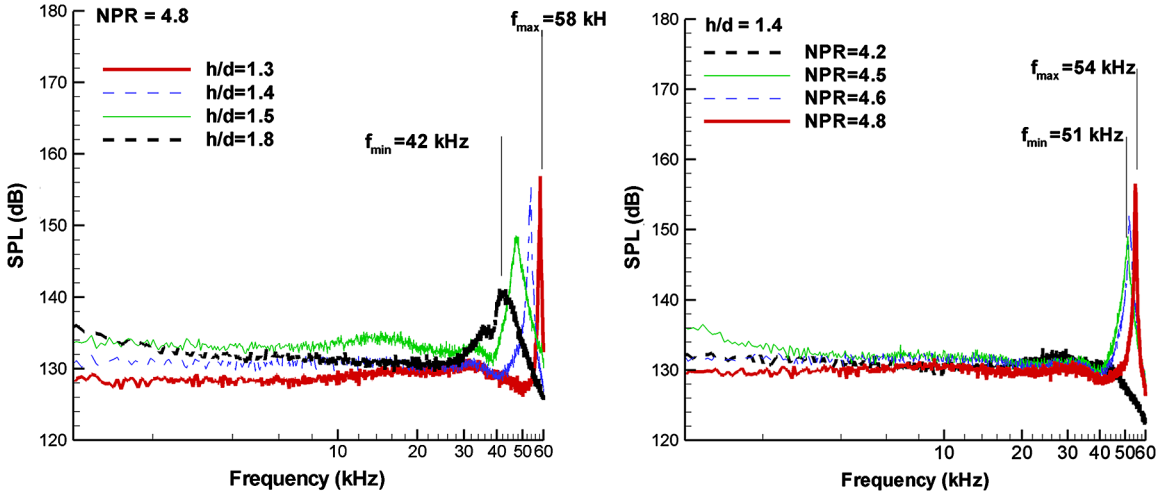

a) Fixed *NPR*, *h/d* variation b) Fixed *h/d*, *NPR* variation

Fig. 8 Pressure spectra for microactuator with $L/d = 1$, where NPR and h/d are varied: a) h/D varied at NPR = 4.8 and b) NPR varied at $h/d = 1.4$.

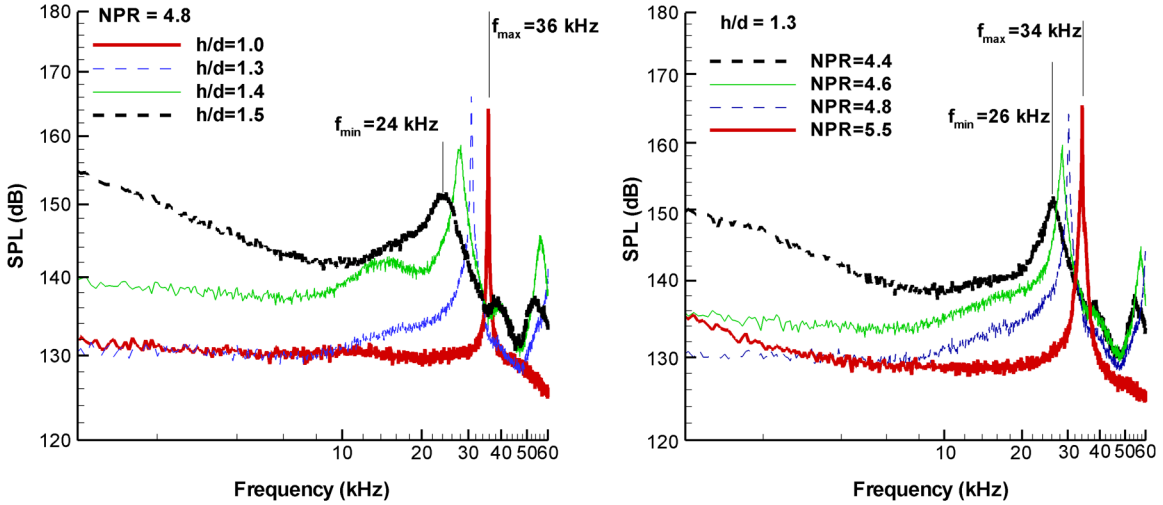

a) Fixed *NPR*, *h/d* variation b) Fixed *h/d*, *NPR* variation

Fig. 9 Pressure spectra for microactuator with $L/d = 2$, where NPR and h/d are varied: a) h/D varied at NPR = 4.8 and b) NPR varied at $h/d = 1.3$.

1.0 to 1.5 has resulted in a frequency response of 36 to 24 kHz with discrete frequency amplitudes of 162 and 150 dB, respectively. Similarly, increasing the NPR from 4.4 to 5.5 (Fig. 9b) shifts the frequency from 26 to 34 kHz while increasing the peak amplitude by roughly 15 dB. The frequency range is further reduced to 14–24 kHz for a longer cavity length $L/d = 3$ (Fig. 10). A closer look at these spectra also reveals that the large-amplitude discrete tones are associated with lower broadband unsteadiness, whereas the spectra consisting of higher broadband levels have lower-amplitude discrete tones. This indicates some redistribution of the total energy with these control parameters. This effect needs further exploration and is being presently studied. Based on the above experiments, the frequency of a microactuator and its relation to the geometrical parameters was established. It was anticipated that $L/d = 5$ will result in a frequency range of 6–12 kHz, suitable for the applications of our interest. A microactuator with $L/d = 5$ was then fabricated and tested over a range of NPR = 4.5 to 5.5, where the h/d was varied from 1.3 to 1.8; these results are shown in Fig. 11.

As we hoped, the spectra show dominant tones in a frequency range of 6–11 kHz, with flow characteristics very similar to those of shorter cavities discussed earlier.

In all of the experiments discussed so far, unsteady pressure measurements were obtained with the Kulite probe placed normal to the jet axis. A few tests were conducted with a probe placed parallel to the unsteady microjet (Fig. 12a), in which the microjet plume just grazes this sensor. These spectra are compared in Fig. 12b. These tests were conducted in part to verify that the fluctuations measured by the Kulite probe were not in fact due to resonance induced by impingement on the probe itself. As seen here, peaks are observed at the same frequency in both cases. However, as expected, the amplitudes are lower for the tangential probe. These results verify that the unsteady microjet flow measured by the Kulite is due to the aeroacoustic coupling within the actuator which significantly enhances the unsteady component of the supersonic flow issuing from these actuators.

The results obtained by varying geometric and flow parameters are summarized in Fig. 13 which shows a variation of the peak frequency as a function of L/d, for a range of h/d and NPR variations. As seen here, by changing the cavity length, L/d from 1 to 5, the resonance frequency of the actuator can be shifted from ~50 kHz to ~4 kHz. For a given actuator design, i.e., fixed L/d, very small change in h/d (open symbols) and/or NPR (filled symbols) one can sweep or tune the actuator frequency over a large range ($\Delta f_{\text{actuator}} \sim$ 5–20 kHz).

Using the trends summarized in Fig. 13, one may design an actuator in the frequency range of roughly 1–60 kHz (the upper limit has not been explored to date), the frequency of which can be tuned by fine control knobs (h/d and NPR) around the design envelop frequency based on L/d. A closer look at the results in Fig. 13 show

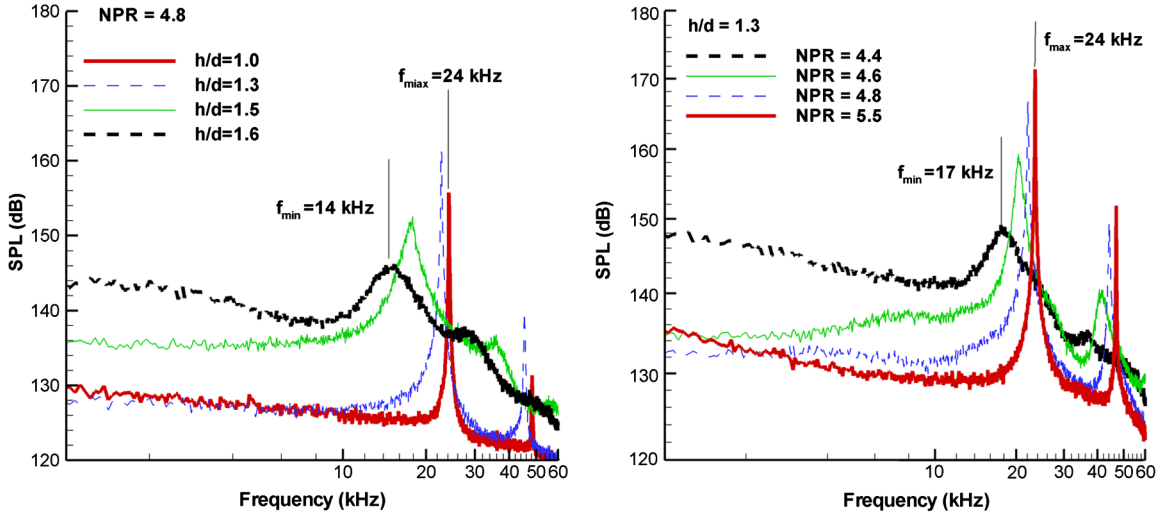

a) Fixed *NPR*, *h/d* variation

b) Fixed *h/d*, *NPR* variation

Fig. 10 Pressure spectra for microactuator with $L/d = 3$, where NPR and h/d are varied: a) h/D varied at NPR $= 4.8$ and b) NPR varied at $h/d = 1.3$.

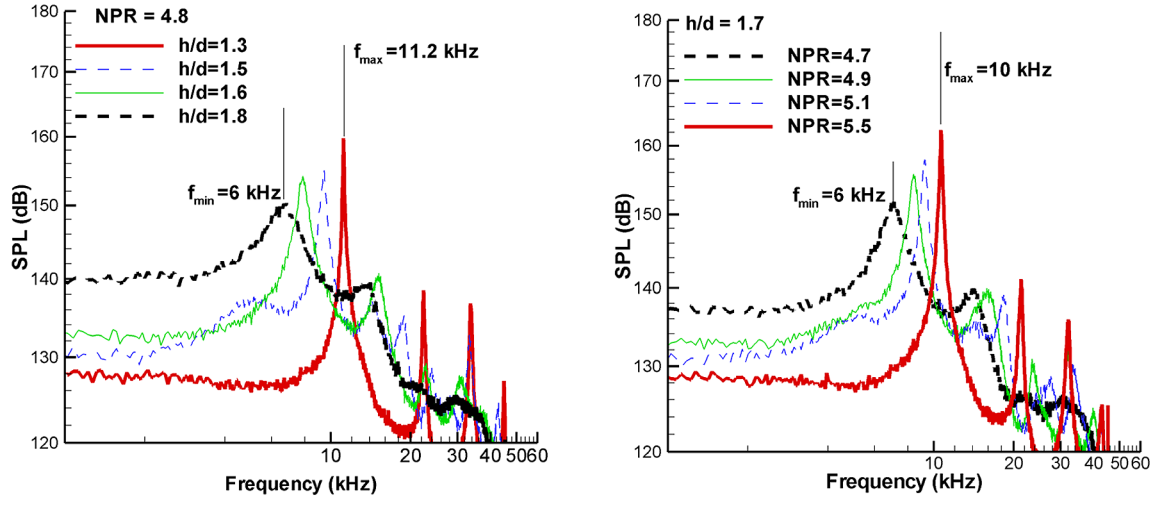

a) Fixed *NPR, h/d* variation

b) Fixed *h/d, NPR* variation

Fig. 11 Pressure spectra for microactuator with $L/d = 5$, where NPR and h/d are varied: a) h/D varied at NPR $= 4.8$ and b) NPR varied at $h/d = 1.7$.

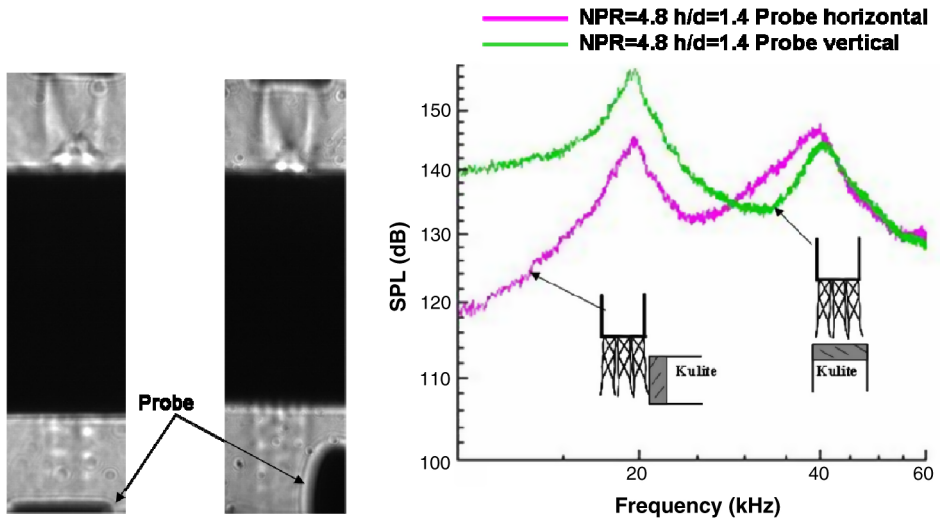

a) Probe location b) Spectra

Fig. 12 Effect of probe direction on pressure spectra.

that an h/d variation from 1.0 to 1.7, at a constant NPR, has resulted in a decrease in the frequency, a trend similar to that of variable L. This suggests that jet column length may be a better combined parameter that describes the effect of both h/d and L/d. Hence, we define a new variable $H = h + L$. This parameter H represents the total length of the jet column, from the source nozzle exit to the bottom of the cavity. The results shown in Fig. 13 are replotted in dimensionless parameters, Strouhal number St_{ideal} and H/d. For St_{ideal}, the actuator frequency is non dimensionalized using the ideally expanded jet velocity based on the primary source jet NPR as

$$St_{\text{ideal}} = fd/U_{\text{ideal}} \tag{1}$$

In Eq. (1) f is the frequency of the actuator, d is source jet diameter and U_{ideal} is the ideally expanded jet velocity of the underexpanded source jet. Interestingly, these new variables collapse the data reasonably well into a single curve, as seen in Fig. 14. The collapsed curve is approximated by the correlation

$$St_{\text{ideal}} = 0.4(H/d)^{-1.45} \tag{2}$$

Rewriting Eq. (2) in terms of NPR results in

$$f = \frac{0.4}{d}\left(\frac{2}{\gamma - 1}((\text{NPR})^{\frac{\gamma-1}{\gamma}} - 1)\right)^{1/2}\sqrt{\gamma R T_o (\text{NPR})^{\frac{1-\gamma}{\gamma}}}(H/d)^{-1.45} \tag{3}$$

where γ is the specific heat ratio, T_o is the stagnation temperature of the source jet and R is the universal gas constant.

This correlation can in turn be used as a guide for designing actuators with a high bandwidth and tunable frequency. Microjet actuator arrays designed using the above approach can potentially be used for a number of supersonic (and subsonic) flow control applications which require high unsteady and mean components, such as those produced herein.

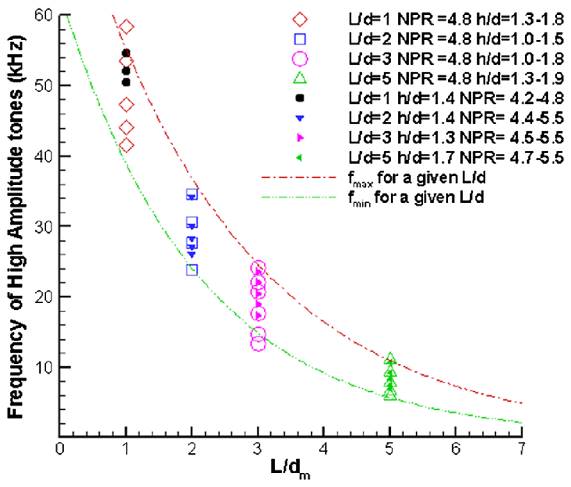

Fig. 13 Summary of actuator performance in terms of geometric, L/D and h/D, and flow parameters.

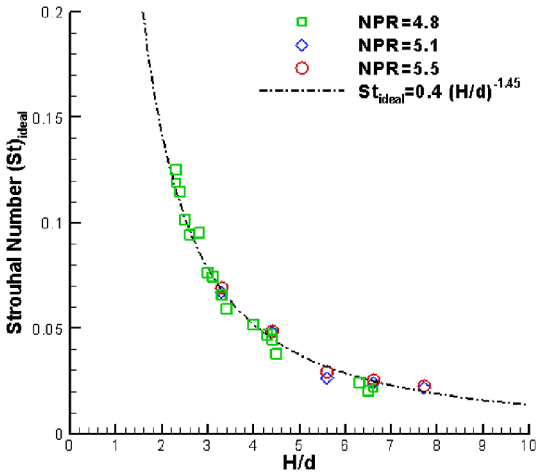

Fig. 14 Actuator dynamics in nondimensional frequency and modified parameter H/d, where $H = h + L$.

VII. Comparison of Present Microactuator Properties with Other Designs

As noted in the introduction, a number of past studies used flow resonance phenomena to design actuators for various flow control applications. In the current actuator design we have a supersonic microjet entering a partially open cavity. Since a Hartmann tube is a closed cavity and closely resembles the present geometry, it may be useful to compare the predictions of Hartmann and Trolle [22] and other actuator designs based on Hartmann's principles with the present actuator. Figure 15 shows the variation of the peak frequencies as a function of jet column length H/d (where $H = L + h$) for the present microactuator along with the data from literature. Here, we compare the present microactuator frequency with Hartmann predictions and the experimental data of Raman and

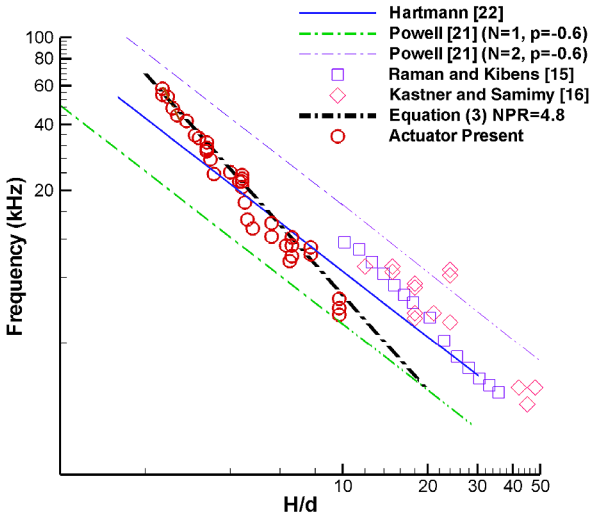

Fig. 15 Comparison of microactuator frequency with other designs and predictions.

Kibens [15] and Kastner and Samimy [16]. Both of these designs were based on the original Hartmann approach. In the plot in Fig. 15, the results from the present actuator are shown as circles, while data from Raman and Kibens [15] and Kastner and Samimy [16] are shown as polygons.

In addition, the frequency predictions of Hartmann [22] are shown as a solid line. It is clear from this plot that Kastner and Samimy's [16] and Raman and Kibens's [15] actuator designs, which are closely based on the Hartmann approach, produced tones of frequencies that agree reasonably well with Hartmann's predictions, in particular for longer cavity lengths. In contrast, the microactuator frequencies, while similar in magnitude, exhibit a different H/d dependence than predicted by the Hartmann correlation.

Another comparison is made with Powell's feedback correlation [20] (shown as dash-dot lines) that predicts the frequency of impinging or hole tones. The rationale behind this comparison is the similarity between these two flow phenomena. In the current actuator design, the primary jet is impinging on a flat surface, the bottom of cavity, with a number of orifices in it, resembling an impinging-jet flow. In addition, as seen in Fig. 4, the shear layer of the actuator source jet grazes the edges of the cylindrical cavity resembling a hole tone configuration, that may also enhance the feedback-loop-driven instabilities creating unsteadiness in the main jet. This comparison reveals that the actuator frequency falls within the first and second mode of Powell's prediction assuming a phase lag of −0.6. It is worth noting that, with an appropriate choice of a phase lag value, the Hartman prediction and Powell's correlation collapse to one single line. This points toward the influence of feedback-loop-driven instabilities in both of these configurations. In summary, although the present flow displays trends similar to feedback-driven flows examined by Hartmann [22] and Powell [20], it does not agree with either. This is because it is likely a combination of a number of flow resonance phenomena and is better captured by Eqs. (2) and (3).

VIII. Microactuator Amplitude: A Parametric Study

For any actuator system, the amplitude of unsteadiness is as important as its frequency response. The total energy in the unsteady component of the microactuator flow can be captured by the rms of the total pressure measured, P_{rms}. In the following, we describe how the geometric and flow parameters affect the unsteady amplitude of the present microactuator system.

A. Effect of h/d

At a fixed NPR (=4.8), the variation of P_{rms} with h/d for different cavity lengths is shown in Fig. 16a. It is observed that initially an increase in h/d results in an increase in P_{rms}. Beyond a threshold h/d, P_{rms} remains nearly constant over significant a range of h/d, decreasing at larger values. For example, at $L/d = 1$, the P_{rms} is 144 dB at $h/d = 0.75$, it reaches nearly 168 dB at $h/d = 1.1$ and remains nearly constant up to $h/d = 1.6$, it then decays to 158 dB at higher h/d values. As seen in Fig. 16a, this entire variation occurs within an h/d range of 1 to 1.6, a change of only 0.6 mm, and is seen for all the cavity lengths examined. This suggests the existence of a region in which the flow is particularly unsteady and in which the instabilities are amplified: i.e., a region of instability (ROI).

An examination of the schlieren images, similar to those shown in Figs. 6 and 7, corresponding to this ROI range of h/d, reveals that for most of these unstable cases, the cavity entrance is in the compression region of the shock cell structure of the source jet where the local static pressure has begun to increase due to the compression fans in the shock cells. Hence, in addition to the cavity diameter being such that its edges graze the source jet shear layer, the cavity entrance should be located in the compression region of the source jet. This placement with respect to the source jet flowfield leads to large oscillations in the source jet and its Mach disk as seen in Fig. 7. This in turn provides the unsteady source flow/function for the actuator cavity.

Figure 16b shows a variation of P_{rms} with jet column length H/d, where $H = h + L$. Using this variable, which accounts for the length of the cavity, L and h/d, the dependence of P_{rms}, on the total actuator length is more systematically and more clearly revealed. These results once again confirm that there is a range of h/d over which the unsteadiness levels are high for all cases of cavity lengths (L) used in this study. It is also worth noting that while the unstable frequencies change by nearly an order of magnitude between the actuator with the

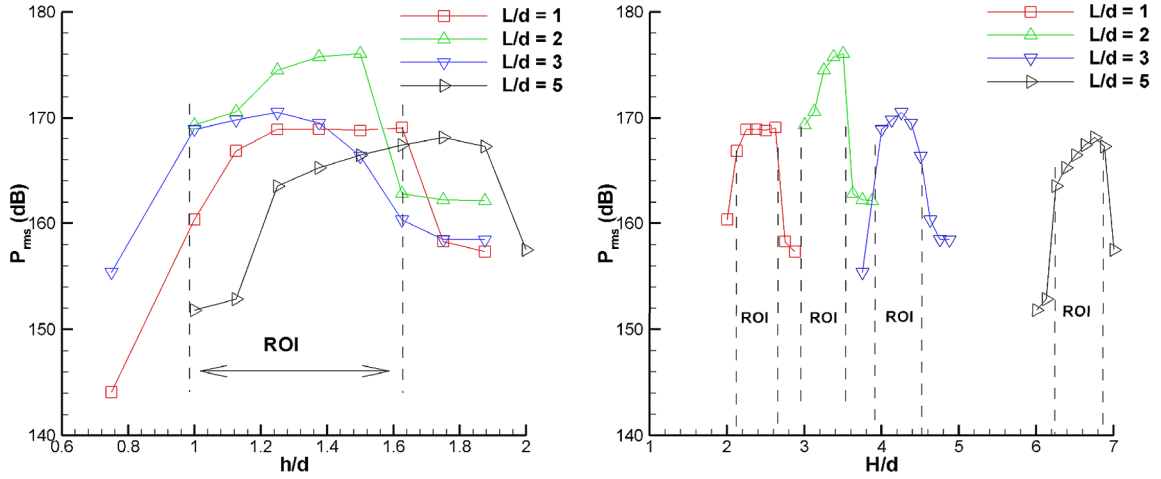

a) Effect of *h/d* **b) Effect of *H/d***

Fig. 16 Unsteady amplitude variation as a function of geometric parameters for a fixed NPR = 4.8.

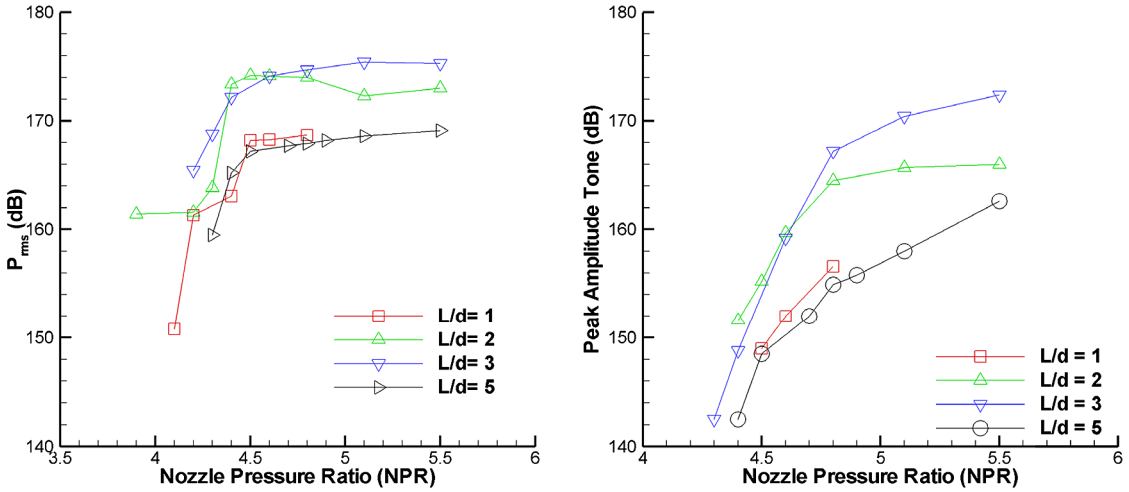

a) P_{rms} b) Tonal amplitude

Fig. 17 Effect of nozzle pressure ratio on flow unsteadiness of microactuator.

shortest cavity ($L/d = 1$) and the longest cavity ($L/d = 5$), the total energy in the unsteady component, i.e., P_{rms}, is relatively constant over the ROI.

While discussing the pressure spectra of the microactuator flow (Figs. 8–11) the emergence of distinct, sharp frequency tones when h/d is varied from 1.0–1.6 was observed. It was noted that high P_{rms}, levels in the same h/d range. It is clear (and perhaps obvious) that the discrete peaks in the pressure spectra, which are indicative of significant unsteadiness, are responsible for the high P_{rms}. The conclusion is that for a sufficiently high NPR, there exists a region of instability within which the variations of h/d give rise to highly unsteady secondary jets with energy concentrated in a limited frequency range. Furthermore, the dominant frequency range for a fixed NPR can be controlled by selecting the appropriate h/d and cavity length L.

B. Effect of NPR

The variation of P_{rms} with nozzle pressure ratio (NPR) is shown in Fig. 17a. In the present experiments, at a fixed value of L/d and h/d (corresponding to highly unsteady flow), the NPR is varied from 4 to 5.5. It is observed that at each L/d, once NPR is increased above 4.2, there is a sharp increase in OASPL. However, this value saturates beyond NPR = 4.5 over the range of conditions tested. This once again suggests the possibility of a region of instability leading to high-amplitude unsteadiness. To further understand the effect of NPR, the peak tonal amplitude is shown in Fig. 17b. It is observed that discrete measurable tones are observed in the spectra beyond NPR = 4.2 and their amplitude increases with increasing NPR. These results confirm that although increasing NPR (beyond 4.5) increases the peak tonal amplitude, the overall unsteadiness in the microactuator system remains nearly constant.

IX. Conclusions

There exists a significant need for high-momentum high-bandwidth microactuators for various high-speed applications, such as jet noise and cavity flows. In this paper, we describe a systematic approach for designing microactuators with high unsteady and mean momentum efflux. Beginning with a simple configuration, i.e., supersonic impinging microjets, we systematically add more complexity to the actuator design, resulting in higher but predictable and controllable unsteady output, to finally arrive at an actuator configuration that provides the desired flow properties. Our first-generation actuator design consists of a primary source jet, incident upon a cylindrical cavity. The lower surface of this cavity contains micronozzles through which the unsteady microjets issue. The results clearly show that the microjets produced by this actuator possess very high mean momentum (they are supersonic for most cases, with velocity of greater than 300 m/s) as well as a very significant unsteady component (50–100 m/s). Using this design, experiments were conducted over a large range of parameters, in terms of cavity length, source jet NPR, and source jet impingement distance. The results unequivocally demonstrate the ability to vary the frequency and the perturbation amplitude of the unsteady microjets issuing from this actuator. By varying the dimensions of the actuator by only a few hundred microns, we are able to finely sweep the frequency of the unsteady component over intervals of 5–20 kHz. We have provided a simple design criterion to develop any actuator over the frequency range of roughly 1–60 kHz by suitably selecting the geometric parameters (we believe that higher frequencies are also possible). The ability to produce unsteady flow with significant mean and unsteady components, where the dynamic range can be easily varied makes these actuators promising for a number of high and low speed flow control applications. The notable characteristics of this design are its simplicity, robustness, scalability and the flexibility in controlling the frequency and amplitude suitable for the application of interest.

Acknowledgments

The authors would like to thank Florida Center for Advanced Aero-Propulsion and the U.S. Air Force Office of Scientific Research for the financial support for this research.

References

[1] Zhuang, N., Alvi, F. S., Alkislar, M. B., and Shih, C., "Supersonic Cavity Flows and Their Control," *AIAA Journal*, Vol. 44, No. 9, 2006, pp. 2118–2128. doi:10.2514/1.14879

[2] Ukeiley, L., Sheehan, M., Coiffet, F., Alvi, F. S., Arunajatesan, S., and Jansen, B., "Control of Pressure Loads in Geometrically Complex Cavities," *Journal of Aircraft*, Vol. 45, No. 3, 2008, pp. 1014–1024. doi:10.2514/1.33324

[3] Krothapalli, A., Rajkuperan, E., Alvi, F. S., and Lourenco, L., "Flow Field and Noise Characteristics of a Supersonic Impinging Jet," *Journal of Fluid Mechanics*, Vol. 392, 1999, pp. 155–181. doi:10.1017/S0022112099005406

[4] Alvi, F. S., Shih, C., Elavarasan, R., Garg, G., and Krothapalli, A., "Control of Supersonic Impinging Jet Flows Using Supersonic Microjets," *AIAA Journal*, Vol. 41, No. 7, 2003, pp. 1347–1355. doi:10.2514/2.2080

[5] Kumar, R., Lazic, S., and Alvi, F. S., "Control of High-Temperature Supersonic Impinging Jets Using Microjets," *AIAA Journal*, Vol. 47, No. 12, pp. 2800–2811. doi:10.2514/1.39061

[6] Ro, I. P., and Loh, G. B., "Feasibility of Using Ultrasonic Flexural Waves as a Cooling Mechanism," *IEEE Transactions on Industrial Electronics*, Vol. 48, No. 1, 2001, pp. 143–150.

doi:10.1109/41.904574
[7] Sfeir, A. A., "Investigation of Three Dimensional Turbulent Rectangular Jets," AIAA Paper 1185, 1978.
[8] Sforza, P. M., Steiger, M. H., and Trentacoste, N., "Studies on Three Dimensional Viscous Jets," *AIAA Journal*, Vol. 4, No. 5, 1966, pp. 800–806.
doi:10.2514/3.3549
[9] Schadow, K. C., Gutmark, E. J., Wilson, K. J., and Smith, R., "Non Circular Inlet Duct Cross-Section to Reduce Combustion Instabilities," *Combustion Science and Technology*, Vol. 73, No. 4, 1990, pp. 537–553.
doi:10.1080/00102209008951669
[10] Zaman, K. B. M. Q., Reeder, M. F., and Samimy, M., "Control of an Axisymmetric Jet Using Vortex Generators," *Physics of Fluids*, Vol. 6, No. 2, 1994, pp. 778–793.
doi:10.1063/1.868316
[11] Reeder, M., and Samimy, M., "The Evolution of a Jet with Vortex Generating Tabs: Real Time Visualization and Quantitative Measurements," *Journal of Fluid Mechanics*, Vol. 311, 1996, pp. 73–118.
doi:10.1017/S0022112096002510
[12] Cattafesta, L. N., III, Garg, S., Choudhari, M., and Li, F., "Active Control of Flow-Induced Cavity Resonance," AIAA Paper 97-1804.
[13] Wiltse, J. M., and Glezer, A., "Manipulation of Free Shear Flows Using Piezoelectric Actuators," *Journal of Fluid Mechanics*, Vol. 249, 1993, pp. 261–285.
doi:10.1017/S002211209300117X
[14] Amitay, M., Kibens, V., Parekh, D. E., and Glezer, A., "Flow Reattachment Dynamics over a Thick Airfoil Controlled by Synthetic Jet Actuators," AIAA Paper 99-1001.
[15] Raman, G., and Kibens, V., "Active Flow Control Using Integrated Powered Resonance Tube Actuators," AIAA Paper 2001-31330.
[16] Kastner, J., and Samimy, M., "Development and Characterization of Hartmann Tube Fluidic Actuators for High-Speed Flow Control," *AIAA Journal*, Vol. 40, No. 10, 2002, pp. 1926–1934.
doi:10.2514/2.1541
[17] Dziuba, M., and Rossmann, T., "Active control of a Sonic Transverse Jet in a Supersonic Cross Flow Using a Powered Resonance Tube," AIAA Paper 2005-897.
[18] Lou, H., Alvi, F. S., and Shih, C., "Active and Adaptive Control of Supersonic Impinging jets," *AIAA Journal*, Vol. 44, No. 1, 2006, pp. 58–66.
doi:10.2514/1.13347
[19] Phalnikar, K. A., Kumar, R., and Alvi, F. S., "Experiments on Free and Impinging Supersonic Microjets," *Experiments in Fluids*, Vol. 44, 2008, pp. 819–830.
doi:10.1007/s00348-007-0438-4
[20] Powell, A., "The Sound Producing Oscillations of Round Underexpanded Jets Impinging on Normal Plates," *Journal of the Acoustical Society of America*, Vol. 83, No. 2, 1988.
[21] Powell, A., "On Edge Tones and Associated Phenomena," *Acoustica* Vol. 3, 1953.
[22] Hartmann, J., and Trolle, B., "A New Acoustic Generator," *Journal of Scientific Instruments*, Vol. 4, No. 4, 1927, pp. 101–111.
doi:10.1088/0950-7671/4/4/303

M. Glauser
Associate Editor